PROCEEDINGS OF SCIENCE

Recent results from CMS

Marco Pieri *†
University of California, San Diego
E-mail: Marco.Pieri@cern.ch

The CMS physics results obtained by summer 2011 will be reported. The CMS detector at LHC collected data at 7 TeV centre-of-mass energy in 2010. During 2011 the LHC luminosity increased up to $3 \times 10^{33}\text{cm}^{-2}\text{s}^{-1}$. Many QCD and electroweak measurements have been carried out. No new particles were detected up to a mass of O(1 TeV) and stringent limits have been derived. The 95% excluded Higgs boson mass range has been further extended compared to the LEP and Tevatron results. The Heavy Ion Physics program of LHC allowed CMS to study the properties of quark gluon plasma produced in Pb-Pb collisions.

10th International Symposium on Radiative Corrections (Applications of Quantum Field Theory to Phenomenology)
September 26-30, 2011
Mamallapuram, India

*Speaker.
†for the CMS Collaboration.

PoS(RADCOR2011)002

1. Introduction

The Compact Muon Solenoid (CMS) [1] is one of the two general-purpose detectors operating at the Large Hadron Collider (LHC). The main characteristic features of CMS, sketched in Fig. 1, are a large superconducting solenoid magnet, which produces a strong field of 3.8 Tesla, an all silicon precision tracker, a high resolution lead tungstate crystal electromagnetic calorimeter, and a fully hermetic hadronic calorimeter. These components are all contained inside the superconducting solenoid. Outside the solenoid, in the return yoke of the magnet, is located a precision and redundant muon system. The detector has been built and is being operated by the CMS Collaboration that consists of more than 3000 scientists and engineers from 182 Institutes distributed in 39 countries all over the world. LHC started operating in 2009 and the commissioning of the CMS detector for physics started during the first LHC pilot runs at 0.9 and 2.36 TeV collision energies and continued in 2010 after the first run at 7 TeV centre-of-mass energy.

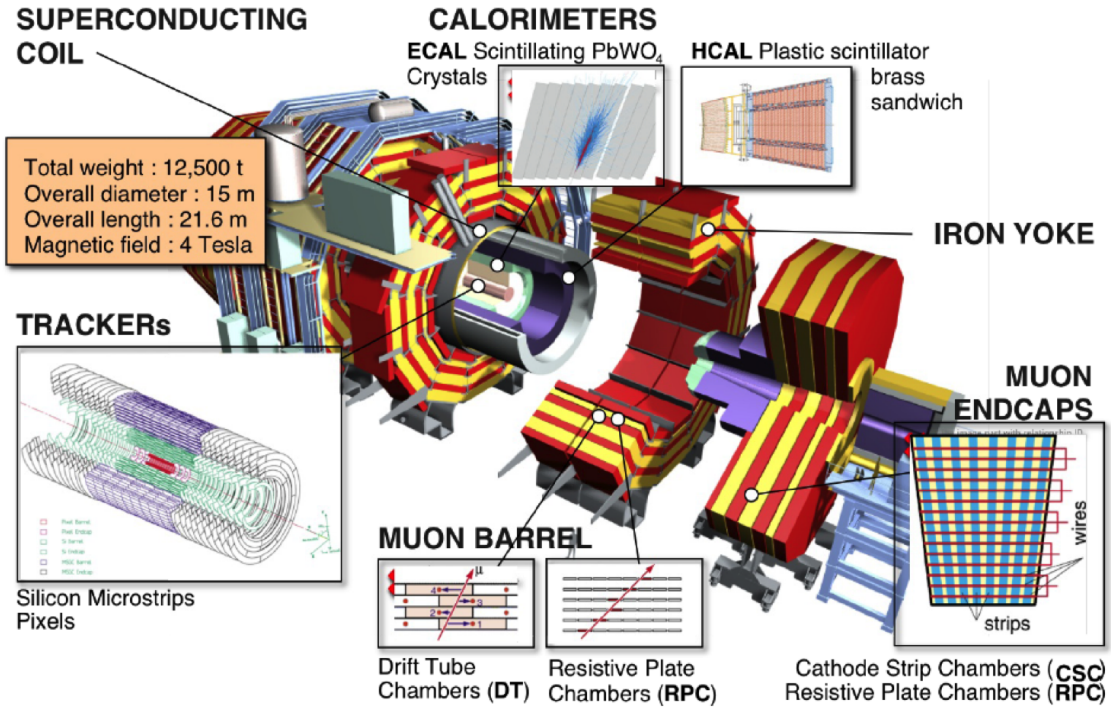

Figure 1: Sketch of the CMS detector.

In CMS we developed a high performance particle flow algorithm. It combines and links in an optimal way signals detected in the different subdetectors, corresponding to same particle, and provides the event description in form of a list of particles: electrons, muons, charged hadrons, photons and neutral hadrons. The particle flow algorithm brings major improvements in the measurement of τ leptons, jets and missing transverse energy (MET) and is widely used in CMS analysis.

2. CMS data taking

During 2011 the LHC luminosity was initially increased by increasing the number bunches up to 1380 per beam that is the maximum possible with a bunch spacing of 50 ns (the design bunch

spacing of 25 ns may be used in 2012). Near the end of the year the per-bunch luminosity was increased by increasing the bunch intensity and decreasing emittance and β^*.

The maximum luminosity achieved by the end of September 2011 was $3.2 \times 10^{33}\text{cm}^{-2}\text{s}^{-1}$. By the end of September 2011, CMS had recorded 3.3 fb^{-1} out of 3.7 fb^{-1} delivered by the LHC (an efficiency of 90%). Roughly 90% of the recorded data is usable for all physics analysis. The overall status of CMS during the data taking was excellent: all sub-systems had a fraction of operational channels exceeding 98%.

The excellent performance of LHC, and the high instantaneous luminosity reached, caused multiple interactions to occur during each bunch crossing. Near the end of the data taking, a peak number of such pileup events of 15 was observed. Thanks to the excellent tracking and to the event by event pileup subtraction methods, the impact on the analysis of such spurious interactions has been kept to a minimum level.

One of the key features of the CMS experiment is the trigger system. It is based on two levels of triggers: the Level 1 that is implemented in the hardware and the High Level Trigger (HLT). The Level 1 combines information from the calorimeters and muon systems and operates at a maximum rate of 100 kHz. Full events are read out at this rate. They are built and sent to the surface to the High Level Trigger (HLT) farm that filters them using offline type software. The HLT has access to the full event information and runs the standard offline reconstruction with minor modification to optimize the reconstruction speed. The final output to tape is about 300 Hz. The HLT consists of hundreds of independent trigger paths that select events for all analyses using single object triggers, multi-object triggers and different prescaled triggers that are needed for control samples or for analyses that are based on very high rate signals.

3. QCD measurements

The rate of jet production at hadron colliders is extremely high and the inclusive jet production cross section represents one of the basic measurements performed at LHC. Using about 35 pb^{-1} of data the jet transverse momentum spectrum has been measured in the p_T range of 18-700 GeV/c and for rapidities $|y| < 3.0$. Low p_T jets were recorded with a prescaled Minimum Bias trigger, and the measurement is extended to high p_T using single-jet triggers with different prescales. Jets are reconstructed using the anti-k_T algorithm with distance parameter of 0.5 [2]. Fig. 2 shows the inclusive jet cross section [3] and dijet invariant mass distributions [4] measured by CMS and compared to Quantum Chromodynamics (QCD) calculations. Data are found in excellent agreement with QCD predictions.

Many other soft and hard QCD measurements have been carried out and a general agreement with MC predictions has been observed.

3.1 Charged particles angular correlations

One measurement that shows discrepancies with the existing Monte Carlo generators is that of two-particle angular correlations of charged particles. It was measured by CMS in proton-proton (pp) collisions at center of mass energies ($\sqrt{s}$) of 0.9, 2.36 and 7 TeV [5].

This study of short- and long-range correlations in pp collisions at the LHC high energy frontier provides important information for characterizing QCD in this energy regime, especially the

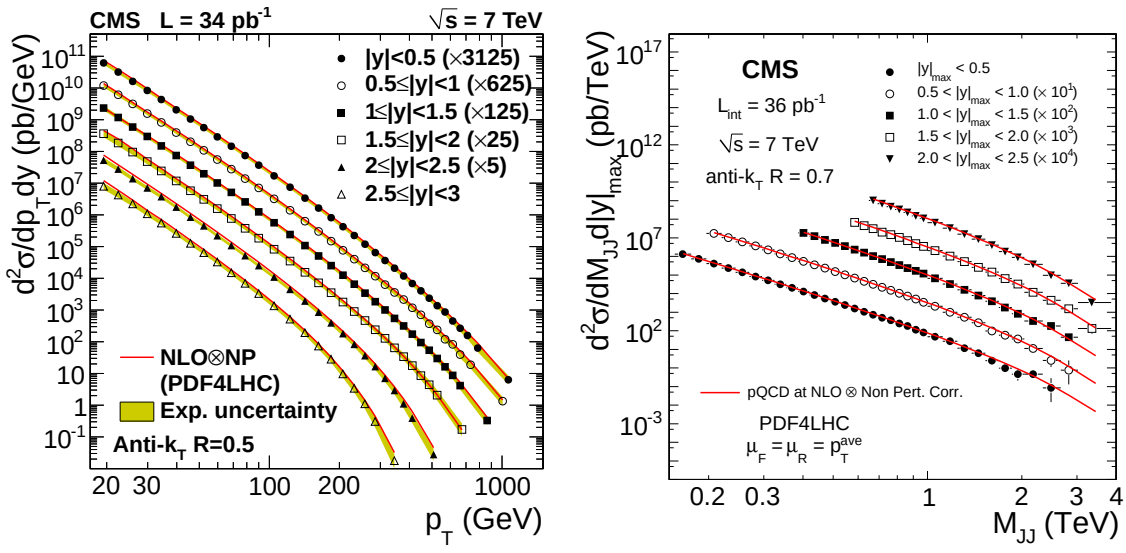

(a) (b)

Figure 2: Comparison between the unfolded measured spectra and the theory predictions for particle-flow jet for inclusive jet cross section (a) and dijet cross section as function of the dijet mass (b). For better visibility the spectra are multiplied by arbitrary factors (indicated in the legend).

mechanism of hadronization and possible collective effects due to the high particle densities. Multiparticle correlations in high energy collisions have been measured previously for a broad range of collision energies and colliding systems with the goal of understanding the underlying mechanism of particle production [6, 7, 8, 9, 10, 11, 12].

We performed two related studies of angular correlations using two-dimensional $\Delta\eta$-$\Delta\phi$ correlation functions [5]: $\Delta\eta$ is the difference in pseudorapidity η ($=-\ln(\tan(\theta/2))$, where θ is the polar angle relative to the beam axis) between the two particles and $\Delta\phi$ is the difference in their azimuthal angle ϕ (in radians). In a first analysis, pp data collected with a minimum bias trigger at 0.9, 2.36, and 7 TeV were used to study short-range correlations ($|\Delta\eta|$ less than $\approx$2). In minimum bias events, a peak with a typical width of about one unit in $\Delta\eta$ is observed.

The long-range structure ($2.0 < |\Delta\eta| < 4.8$) of two-particle correlation functions was examined as a function of charged particle multiplicity and particle transverse momentum. A high-statistics data set of high multiplicity pp events at 7 TeV was used. This sample was obtained thanks to a special high multiplicity trigger.

In current pp Monte Carlo (MC) event generators, the typical sources of such long-range correlations are momentum conservation and away-side ($\Delta\phi \approx \pi$) jet correlations. Measurements at the Relativistic Heavy Ion Collider (RHIC) have revealed that the long-range structure of two-particle angular correlation functions is significantly modified by the presence of the hot and dense matter formed in relativistic heavy ion collisions [12]. Since the particle densities produced in the highest multiplicity pp collisions at LHC energies begin to approach those in high energy collisions of relatively small nuclei such as copper [13], we search for the possible emergence of new features in the two-particle correlation function from high multiplicity pp events. The azimuthal ($\Delta\phi$)

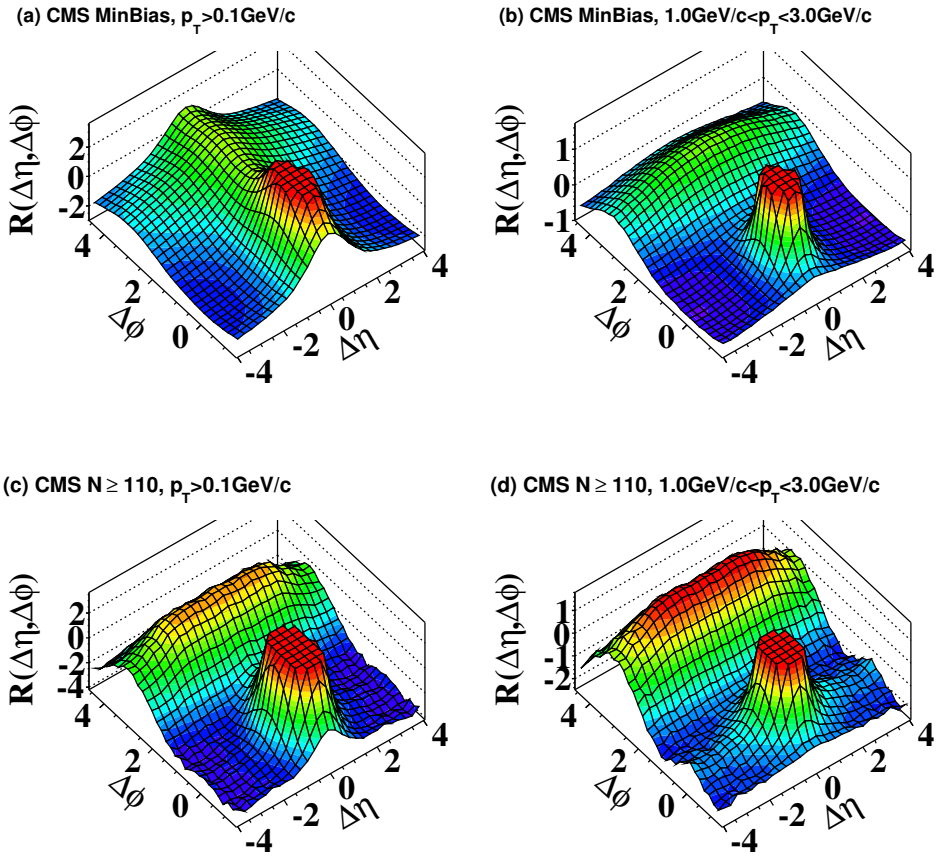

Figure 3: 2-D two-particle correlation functions for 7 TeV pp (a) minimum bias events with $p_T > 0.1\,\text{GeV}/c$, (b) minimum bias events with $1 < p_T < 3\,\text{GeV}/c$, (c) high multiplicity ($N_{\text{trk}}^{\text{offline}} \geq 110$) events with $p_T > 0.1\,\text{GeV}/c$ and (d) high multiplicity ($N_{\text{trk}}^{\text{offline}} \geq 110$) events with $1 < p_T < 3\,\text{GeV}/c$. The sharp near-side peak from jet correlations is cut off in order to better illustrate the structure outside that region.

correlation functions from the large data set at 7 TeV have been studied differentially by binning the events in the observed charged particle multiplicity and by selecting particle pairs in bins of the transverse momentum of the particles.

Fig. 3 qualitatively shows the long-range ridge-like structure at the near-side ($\Delta\phi \approx 0$) that we first observed in pp collisions in events with an observed charged particle multiplicity of $N \approx 90$ or higher. The enhancement in the near-side correlation function is most evident in the intermediate transverse momentum range, $1 < p_T < 3$ GeV/c. In the $2.0 < |\Delta\eta| < 4.8$ range, a steep increase of the near-side associated yield with multiplicity has been found in the data, whereas simulations show an associated yield consistent with zero, independent of multiplicity and transverse momentum. The novel structure resembles similar features observed in heavy ion experiments [12, 14, 15]. However, the physical origin of our observation is not yet understood. Additional characteristics of the high multiplicity pp events displaying this novel feature deserve further studies.

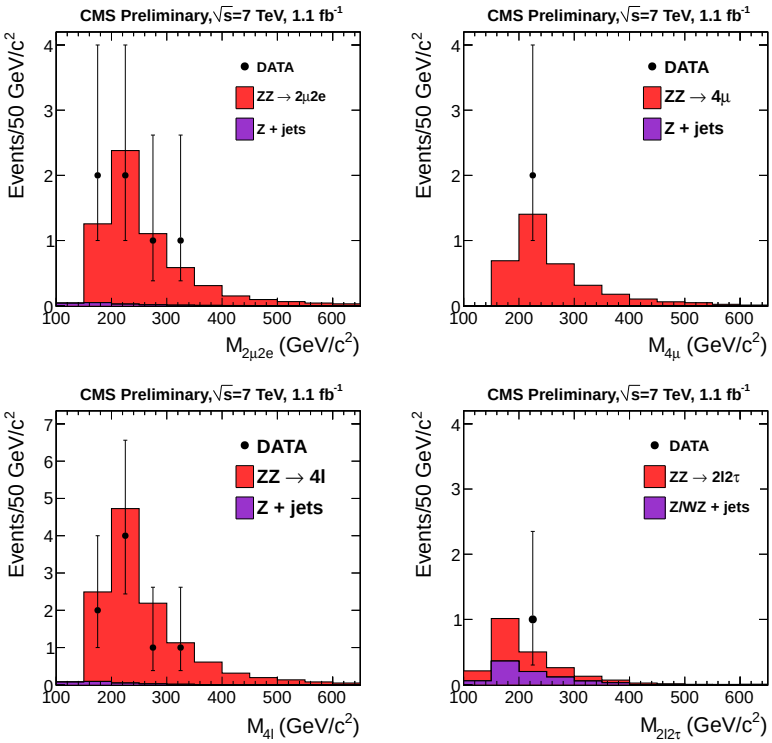

Figure 4: Distributions of the four-lepton reconstructed mass for the 2e2μ and the 4μ final states (top). No events were observed in the 4e final state. The bottom left plot represents the sum of the three 4ℓ channels. The bottom right plot represents the invariant mass of the $2l2\tau$ final state. The data samples correspond to an integrated luminosity of $\mathscr{L} = 1.1$ fb^{-1}.

4. EWK measurements

The first EWK measurements carried out by CMS have been W and Z inclusive production cross sections [16]. They were followed in 2011 by the measurements of diboson production of Vγ [17] and VV [18] production cross sections.

Using an integrated luminosity of 1.1 fb^{-1} recorded in 2010 and 2011 we recently updated the measurement of W^+W^- production and we performed the first measurements of WZ and ZZ production. The W and Z bosons are identified through their decays into electrons and muons for the WW and WZ measurements, and also in tau leptons for the ZZ measurements.

For the measurement of the ZZ cross section, the reconstructed four-lepton invariant mass distribution is shown in Fig. 4 for the different channels and for their combination.

The following values of diboson cross sections have been measured [18]:

$$\begin{aligned}
\sigma(pp \to W^+W^- + X) &= 55.3 \pm 3.3\ (\text{stat.}) \pm 6.9\ (\text{syst.}) \pm 3.3\ (\text{lumi.})\ \text{pb.} \\
\sigma(pp \to WZ + X) &= 17.0 \pm 2.4\ (\text{stat.}) \pm 1.1\ (\text{syst.}) \pm 1.0\ (\text{lumi.})\ \text{pb.} \\
\sigma(pp \to ZZ + X) &= 3.8^{+1.5}_{-1.2}\ (\text{stat.}) \pm 0.2\ (\text{syst.}) \pm 0.2\ (\text{lumi.})\ \text{pb.}
\end{aligned}$$

These measurements are consistent with Standard Model predictions.

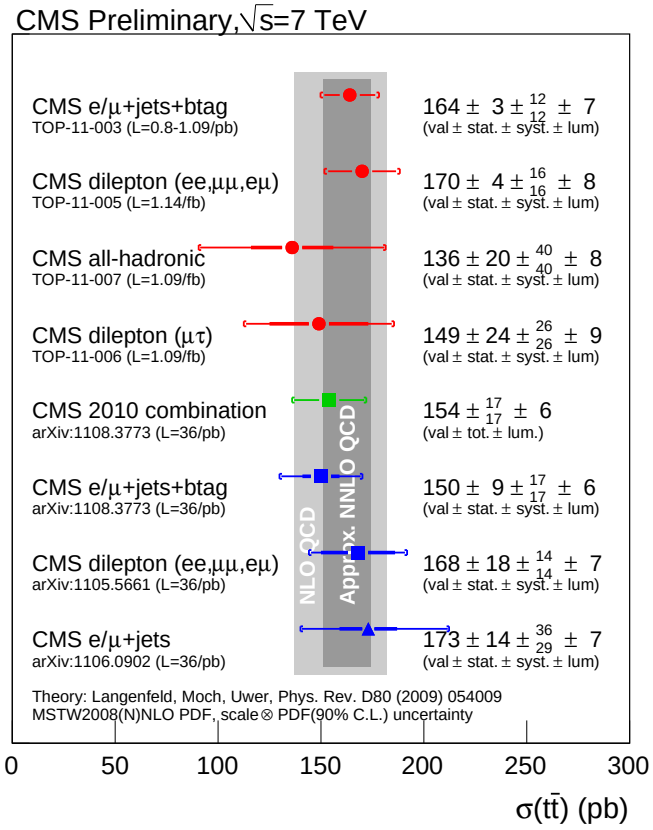

Figure 5: Top pair cross section measurements in different channels.

5. Top measurements

The measurement of the top quark production pair cross-section at the Large Hadron Collider (LHC) is important for various reasons. It probes the dynamics of heavy particle production at a new energy region. New physics can manifest in the production dynamics of top quarks. Within the Standard Model, the top quark decays predominantly to a W boson and a b quark. Depending on the subsequent decays of the W bosons, top quark pairs may decay into final states with zero, one, or two charged leptons from the decays of the W bosons. They are known as ”all hadronic”, ”lepton+jets” and ”dilepton” channels respectively. We have measured the production cross-section of top quark pairs in pp collisions at center-of-mass energy of 7 TeV in different channels [19, 20, 21, 22] and Figure 5 shows the results of the measurements that agree with the SM predictions [23].

We also carried out other measurements in the top sector such as:

- Top charge asymmetry where our measurement is consistent with the Standard Model but with pp collisions at LHC we have lower sensitivity than at a proton-antiproton collider [24].

- Measurement of top-antitop mass difference: We measure 1.2 ± 1.21 (stat) ± 0.47 (syst) GeV/c^2 [25].

- Single top production cross section that we also found consistent with the Standard Model predictions [26].

6. Search for $B_s^0 \to \mu^+\mu^-$ and $B^0 \to \mu^+\mu^-$ decays

The SM-predicted branching fractions, $\mathscr{B}(B_s^0 \to \mu^+\mu^-) = (3.2 \pm 0.2) \times 10^{-9}$ and $\mathscr{B}(B^0 \to \mu^+\mu^-) = (1.0 \pm 0.1) \times 10^{-10}$ [27], are significantly enhanced in several extensions of the SM, although in some cases the decay rates are lowered. For example, in the minimal supersymmetric extension of the SM, the rates are strongly enhanced at large values of $\tan\beta$. Several experiments have published upper limits at 95% confidence level (CL) on these decays: CDF recently reported a new limit of $\mathscr{B}(B^0 \to \mu^+\mu^-) < 6.0 \times 10^{-9}$ and an excess of $B_s^0 \to \mu^+\mu^-$ events, corresponding to $\mathscr{B}(B_s^0 \to \mu^+\mu^-) = (1.8^{+1.1}_{-0.9}) \times 10^{-8}$ [28].

We carried out a simultaneous search for the $B_s^0 \to \mu^+\mu^-$ and $B^0 \to \mu^+\mu^-$ decays [29], using a data sample corresponding to an integrated luminosity of $1.14 \pm 0.07\,\text{fb}^{-1}$, collected in the first half of 2011. An event-counting experiment was performed in dimuon mass regions around the B_s^0 and B^0 masses. To avoid any possible bias, the signal region was kept blind until after all selection criteria were established. The backgrounds are evaluated from the yields measured in data mass sidebands and from Monte Carlo (MC) simulations for rare hadronic two-body B decays.

The $B_s^0 \to \mu^+\mu^-$ branching fraction is measured separately in the barrel and endcap channels from the background-subtracted number of observed $B_{d(s)} \to \mu^+\mu^-$ candidates in the signal window ($5.3 < m_{\mu\mu} < 5.45\,\text{GeV}/c^2$ for B_s^0 and $5.2 < m_{\mu\mu} < 5.3\,\text{GeV}/c^2$ for B^0). Events in the signal window can result from real signal decays, combinatorial background, and "peaking" background from decays of the type $B_{d(s)} \to hh'$, where h, h' are charged hadrons misidentified as muons.

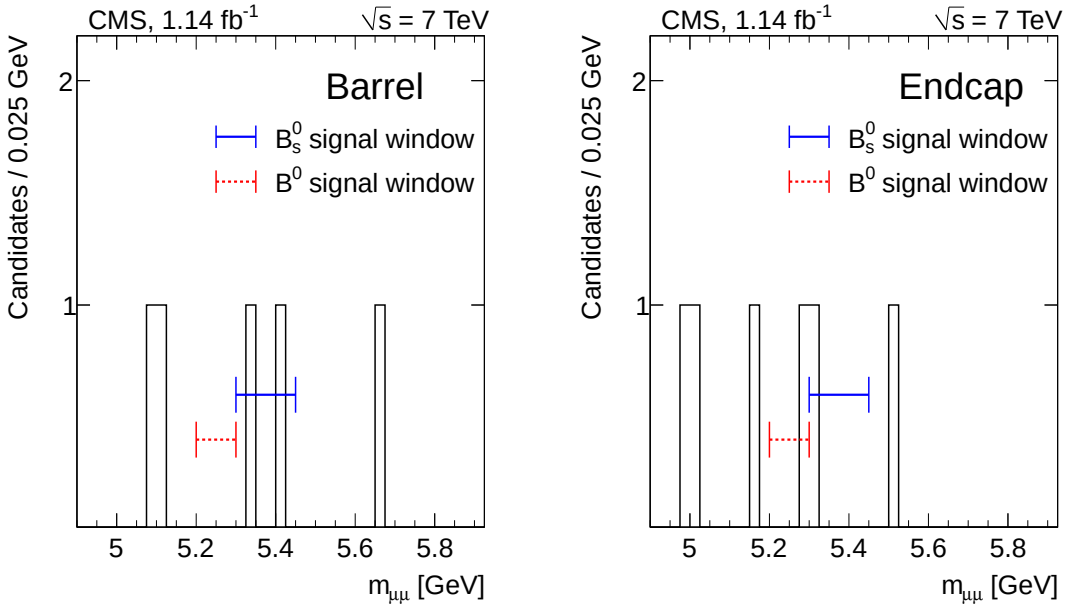

Figure 6: Dimuon invariant mass distributions in the barrel (left) and endcap (right) channels. The signal windows for B_s^0 and B^0 are indicated by horizontal lines.

Figure 6 shows the measured dimuon invariant mass distributions. Three events are observed in the $B_s^0 \to \mu^+\mu^-$ signal windows (two in the barrel and one in the endcap), while only one event is observed in the $B^0 \to \mu^+\mu^-$ endcap channel. This observation is consistent with the SM expectation for signal plus background.

Upper limits are determined starting from the number of observed events in the signal windows, $N_{\rm obs}$.The obtained upper limits on the branching fractions are $\mathscr{B}(B_s^0 \to \mu^+\mu^-) < 1.9 \times 10^{-8}$ (1.6×10^{-8}) and $\mathscr{B}(B^0 \to \mu^+\mu^-) < 4.6 \times 10^{-9}$ (3.7×10^{-9}), at 95% (90%) CL. The median expected upper limits at 95% CL are 1.8×10^{-8} (4.8×10^{-9}) for $B_s^0 \to \mu^+\mu^-$ ($B^0 \to \mu^+\mu^-$). The background-only p value is 0.11 (0.40) for $B_s^0 \to \mu^+\mu^-$ ($B^0 \to \mu^+\mu^-$), corresponding to 1.2 (0.27) standard deviations. The p value is 0.053 when assuming a $B_s^0 \to \mu^+\mu^-$ signal at 5.6 times the SM value, as reported in Ref. [28]. The observed event yields are consistent with those expected from SM processes.

By combining our result with the one obtained by LHCB we obtained a more stringent limit $\mathscr{B}(B_s^0 \to \mu^+\mu^-) < 1.1 \times 10^{-8}$ at 95% C.L. [30].

7. Standard Model Higgs search

The discovery of the mechanism for electroweak symmetry breaking is one of the key goals of the Large Hadron Collider (LHC) physics program. The Minimal Standard Model requires one Higgs doublet and predicts the existence of one scalar Higgs boson. The Higgs boson mass is essentially the only unknown in the model, all other parameters being reasonably well constrained by present measurements. To date, the experimental searches for the Higgs boson have yielded negative results and 95% C.L. limits on its mass have been placed by experiments at LEP, $m_H > 114.4\,\mathrm{GeV}/c^2$ [35], and the Tevatron, $m_H \notin [100, 109]$ and $m_H \notin [156, 177]\,\mathrm{GeV}/c^2$ [36]. Fits of the electroweak precision measurements, that not take into account the direct search results, constrain indirectly the SM Higgs boson mass to be relatively light, $m_H < 158\,\mathrm{GeV}/c^2$ [37].

The CMS Experiment was designed to be able to detect a Higgs boson with a mass ranging from the LEP lower mass bound up to roughly 1 TeV/c^2. Depending on the Higgs boson mass various production mechanisms and decay channels are possible and are searched for. In this note, we report the results of the searches in the channels indicated in Table 1. The analysis strategies are of three types: cut-and-count analyses, analyses of binned distributions, and unbinned analyses tracking individual events and using parametric models of signal and background shapes. The analyzed integrated luminosity varies from channel to channel in the range from 1.1-1.7 fb^{-1}.

The most sensitive channels, important in the theoretically most favoured mass range $M_H < 160\,\mathrm{GeV}/c^2$, briefly described in the following, are:

- $H \to \gamma\gamma$,
- $H \to ZZ \to 4\ell$,
- $H \to WW \to 2\ell 2\nu$.

7.1 $H \to \gamma\gamma$ channel

The Higgs decay branching ratio into $\gamma\gamma$ is rather small, approximately 0.002, for a Higgs boson mass below about 150 GeV/c^2 and becomes negligible for larger masses. This is the most

sensitive channel for masses below approximately 125 GeV/c^2. The signature is two isolated photons which produce a narrow peak above a rather large background mainly composed of irreducible diphoton QCD production and reducible photon plus jet productions where the jet fakes a photon. The Higgs mass resolution is the most important feature of the detectors and the CMS electromagnetic calorimeter that has a resolution of about 1% is very well suited for this analysis.

The photon selection is based on isolation, shower shape and electron rejection and is optimized in different categories because of different background levels. For the CL calculation, events are classified in 8 categories split according to the following features: both photons in barrel or not, both photons unconverted or not and diphoton P_t larger or not than 40 GeV/c.

The confidence level is finally computed using the diphoton mass distribution and estimating the background from the fit to the data sidebands. We found no significant excess in the full mass range [38].

7.2 $H \to ZZ \to 4\ell$ channel

We search in the channels: $H \to ZZ \to 4$ leptons where the 4 leptons can be 4e, 4μ or 2e2μ. This channel has a very clean signature: two pairs of high P_t electrons or muons and at least one pair consistent with the Z mass. A narrow mass peak is expected with a mass resolution of 2-4 GeV/c^2. The expected background is very small and is dominated by the irreducible ZZ to 4 leptons continuum. This channel is sensitive in the mass range 130–600 GeV/c^2 except the region around 160 GeV/c^2 where the Higgs decays are dominated by H $\to$ WW. After selection criteria are applied the expected events from the background are 21.2 ± 0.8 while we observe 21 events in the data with no significant excess [39].

7.3 $H \to WW \to 2\ell 2\nu$ channel

This is the most sensitive channel around 2 M_W ($130 < M_H < 200$ GeV/c^2). The signature is two high P_t isolated leptons + MET. In contrast to the backgrounds, the scalar nature of the Higgs boson and the V-A structure of W decay favour a small opening angle between the 2 charged leptons. The Higgs mass cannot be directly reconstructed and the analysis is a cut and count analysis where the

Table 1: Summary information on the analyses carried out, the integrated luminosity and analysis strategies are indicated.

channel	mass range (GeV/c^2)	luminosity (fb^{-1})	type of analysis
$H \to \gamma\gamma$	110-150	1.7	mass shape (unbinned)
$H \to \tau\tau$	110-140	1.1	mass shape (binned)
$H \to bb$	110-135	1.1	cut&count
$H \to WW \to 2\ell 2\nu$	110-600	1.5	cut&count
$H \to ZZ \to 4\ell$	110-600	1.7	mass shape (unbinned)
$H \to ZZ \to 2\ell 2\tau$	180-600	1.1	mass shape (unbinned)
$H \to ZZ \to 2\ell 2\nu$	250-600	1.6	cut&count
$H \to ZZ \to 2\ell 2q$	226-600	1.6	mass shape (unbinned)

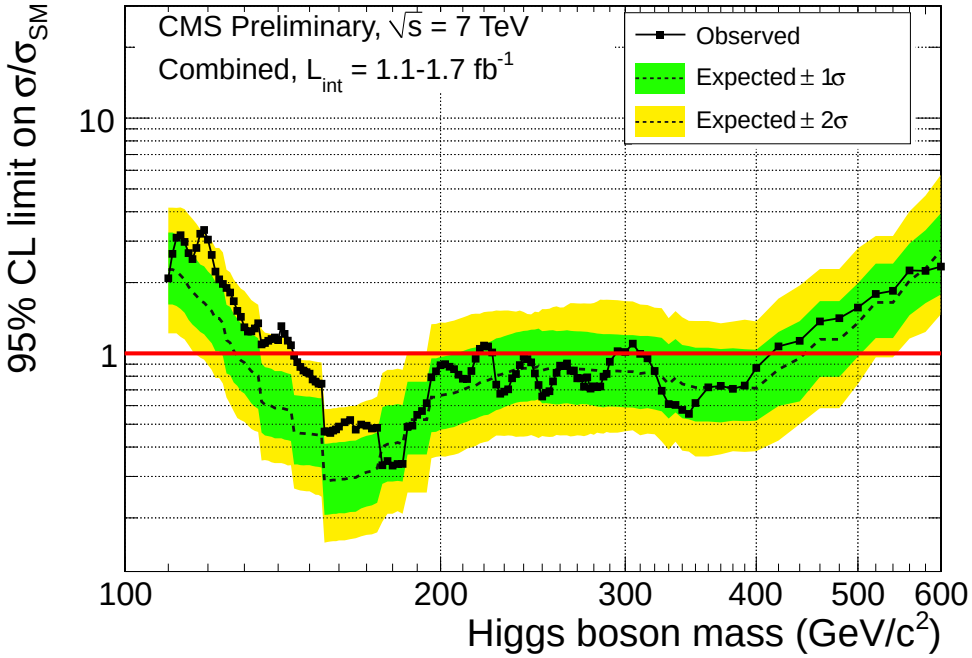

Figure 7: The combined 95% C.L. upper limits on the signal strength as a function of the SM Higgs boson mass in the range 110-600 GeV/c^2. The observed limits are shown by the solid symbols and the black line. The dashed line indicates the median expected limit on μ for the background-only hypothesis, while the green/yellow bands indicate the ranges that are expected to contain 68%/95% of all observed limit excursions from the median.

most crucial aspect is the background estimation that is carried out as much as possible from the data. We found no significant excess in the full mass range [40].

7.4 Higgs search results

None of the searches in the various decay channels show any significant excess of events beyond expected background. Limits on the signal strength modifier, $\mu = \sigma/\sigma_{SM}$, are derived assuming SM cross sections and Branching Ratios. All channels are combined to obtain the final Confidence Level for exclusion/discovery. The results of combining all eight analyses are presented in Figures 7–9 [41].

Fig. 7 shows the 95% C.L. upper limits on the signal strength modifier $\mu = \sigma/\sigma_{SM}$ as a function of the SM Higgs boson mass. We exclude the SM Higgs boson at 95% C.L. in the three mass ranges 145-216, 226-288, and 310-400 GeV/c^2. This substantially reduces the allowed mass range for the SM Higgs boson that has remained unrestricted by the past LEP [35] and ongoing Tevatron [36] direct searches. The expected exclusion, in the absence of a signal, is from 130-440 GeV/c^2. The two gaps between the three excluded mass ranges observed in data are consistent with statistical fluctuations. The individual channel 95% C.L. upper limits on the signal strength modifier $\mu = \sigma/\sigma_{\rm SM}$ as a function of the Higgs boson mass are presented in Fig. 8.

The local p-value as function of the Higgs mass is shown in Fig. 9. The p-value is the estimated probability of upward background fluctuation as high or higher than the excesses observed in data.

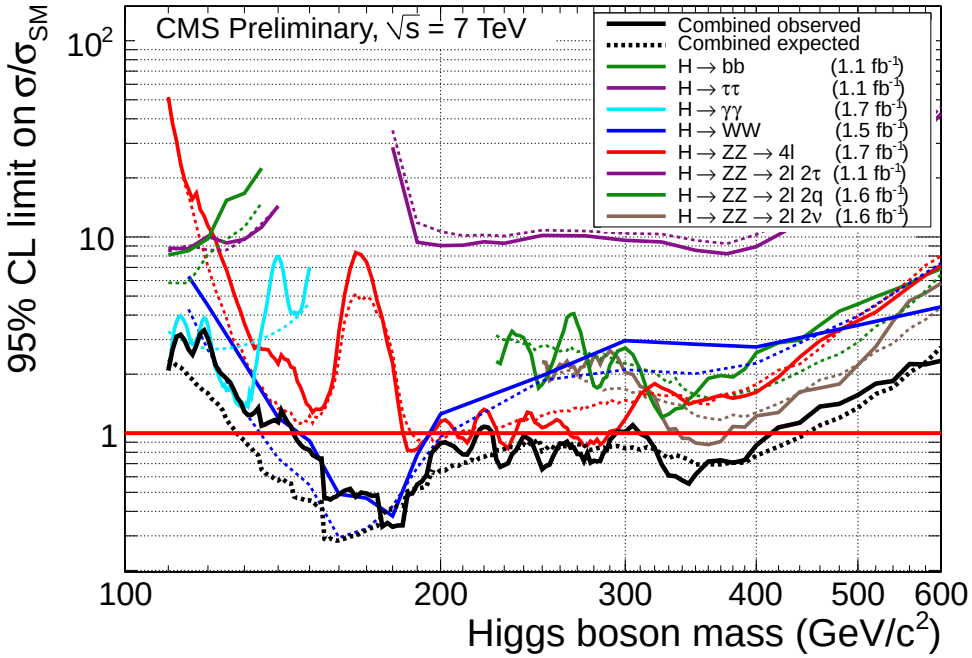

Figure 8: The observed 95% C.L. upper limits on the signal strength modifier $\mu = \sigma/\sigma_{SM}$ as a function of the SM Higgs boson mass in the range 110-600 GeV/c^2 for the eight analyses and their combination. The solid lines show the observed limits, while the dashed lines indicate the median expected assuming the *background-only* hypothesis.

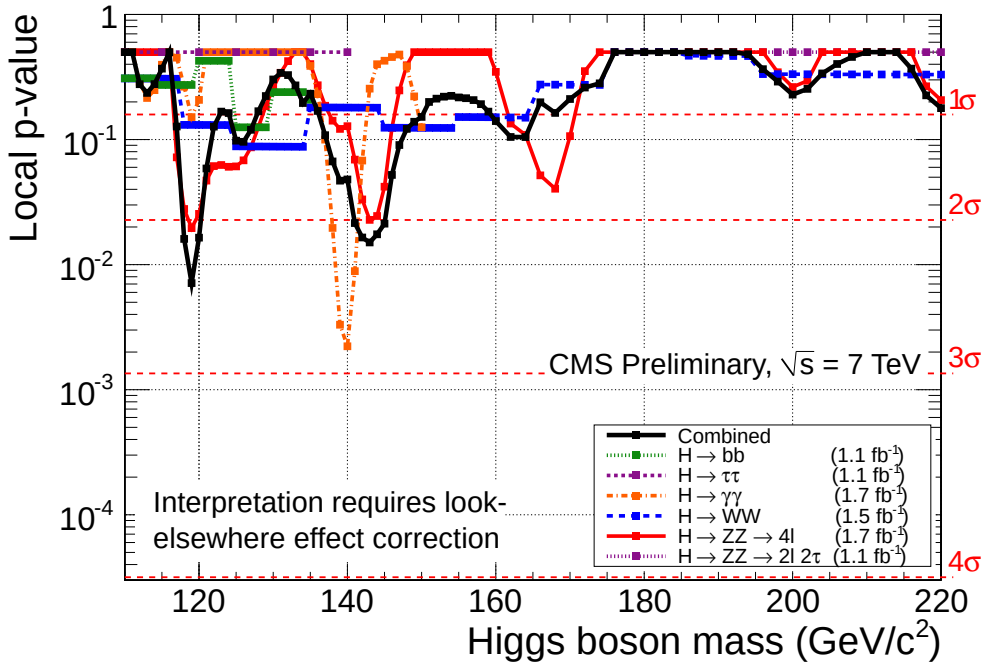

Figure 9: The overall combined *local* p-values (solid black line) and contributions of individual channels entering the combination vs. Higgs boson mass.

After taking into account the look-elsewhere effect that corresponds to the fact that we are searching in a wide mass range, the probability to see an excess at least as large as the one observed in data increases to ~ 0.4.

Overall, the only conclusion we can derive from the present search results are the exclusion limits reported above. More data, including those already collected in 2011 and further expected in 2012, will increase the statistical accuracy of the existing analyses and allow us to introduce further improvements in search strategies and possibly discover the Higgs boson.

8. Other searches

The large increase in CM energy of LHC with respect to the Tevatron expands a lot the reach for the search for new particles. Many types of particles predicted by different theories have been searched for: from Higgs bosons beyond the Standard Model to Supersymmetric partners of the standard particles to more exotic particles such as leptoquarks or microscopic black holes. Unfortunately we found no positive signals and we only obtained new exclusions.

8.1 SUSY searches

The Supersymmetric theory can solve the hierarchy problem of the Standard Model by introducing a large number of supersymmetric particles with the same quantum numbers as the SM particles, but differing by half a unit of spin. If R-parity conservation is assumed, supersymmetric particles are produced in pairs and decay to the lightest supersymmetric particle (neutralino or LSP), leading to a characteristic signature of events with large missing transverse energy. The dominant hard production channels at the LHC would lead to squark-squark, squark-gluino and gluino-gluino pair production. Heavy squarks and gluinos decay into quarks, gluons and other SM particles, as well as neutralinos which escape undetected, leading to final states with several hadronic jets, leptons and large missing transverse energy.

Different searches have been performed using many different topological signatures of SUSY: di-photons and large missing E_t, same sign and opposite sign di-leptons, single leptons and large missing E_t, multi-leptons and fully hadronic final states with large missing E_t. None of these searches has given any hints of production of SUSY particles so far. Limits have been derived and squarks and gluinos up to 1 TeV/c^2 and beyond are excluded at 95% CL.

Fig. 10 shows the 95% C.L. exclusion limits from various analyses in the mSUGRA/CMSSM model [42, 43] produced by these analyses for a particular choice of SUSY parameters of $A_0 = 0$, $\mu > 0$ and $\tan\beta = 10$. Squarks and gluinos up to 1 TeV and beyond are excluded at 95% CL.

8.2 Exotic searches

We searched for many different types of new particles. A full summary of the results can be found at [44].

Here we give an example of the search for narrow resonances in the invariant mass spectrum of dimuon and dielectron final states in event samples corresponding to an integrated luminosity of $1.1\,\mathrm{fb}^{-1}$.

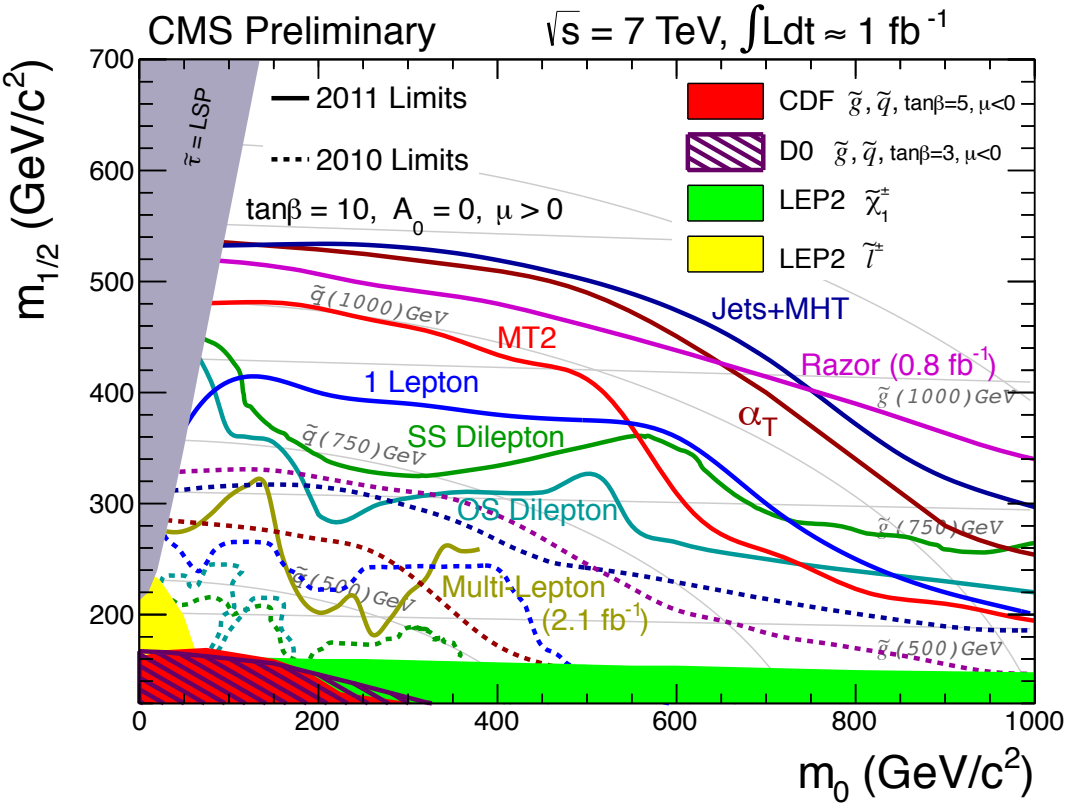

Figure 10: Combined exclusion limits in the mSUGRA/CMSSM m_0, $m_{1/2}$ plane with $\tan\beta = 10$.

The spectra shown in Fig. 11 are consistent with expectations from the Standard Model and upper limits have been set on the cross section times branching fraction for Z′ into lepton pairs relative to standard model Z boson production. Mass limits have been set on neutral gauge bosons Z′ and RS Kaluza–Klein gravitons G_{KK}. A Z′ with standard-model-like couplings can be excluded below 1940 GeV/c^2, the superstring-inspired Z'_ψ below 1620 GeV/c^2, and RS Kaluza–Klein gravitons below 1450 (1780) GeV/c^2 for couplings of 0.05 (0.10), all at 95% CL.

9. Results from the Heavy Ion running

The LHC physics program includes heavy-ion collisions. For a few weeks every year, lead ions are accelerated and collided in the Large Hadron Collider. In November 2010 the Large Hadron Collider (LHC) had its first PbPb collisions produced by the LHC and recorded by the experiments. In about one month CMS collected a total integrated luminosity of $L_{PbPb} = 6.7\ \mu\text{b}^{-1}$ at nucleon-nucleon centre of mass energy $\sqrt{s_{NN}} = 2.76$ TeV.

High-energy collisions of heavy ions allow the study of QCD under extreme conditions of temperature and density. Lattice QCD calculations [46] predict a new form of matter at energy densities above $\varepsilon_{\text{crit}} \approx 1$ GeV/fm^3 consisting of an extended volume of deconfined and chirally-symmetric (bare-mass) quarks and gluons: the Quark Gluon Plasma (QGP) [47, 48, 49, 50]. By

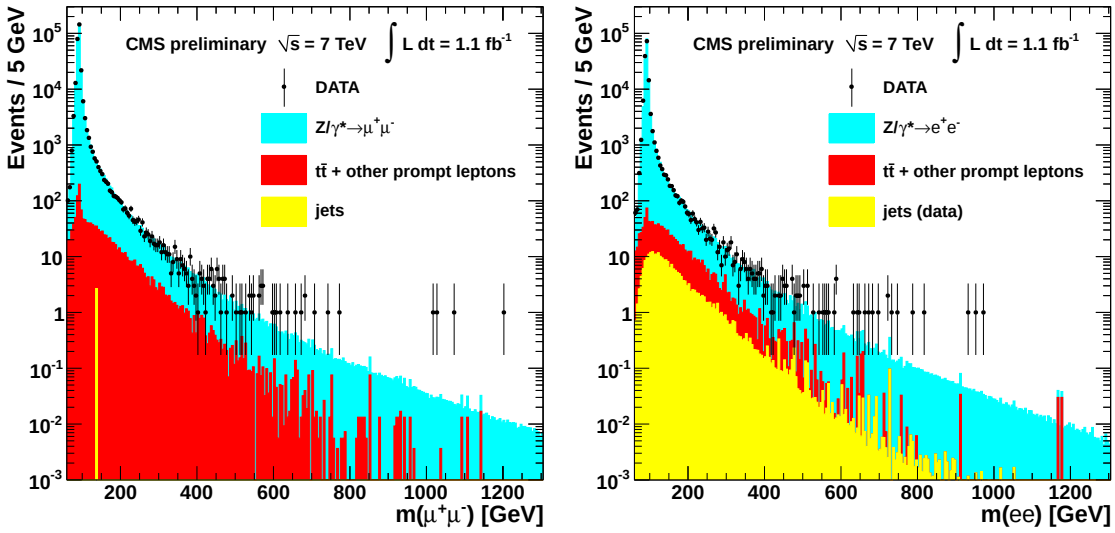

Figure 11: Invariant mass spectrum of $\mu^+\mu^-$ (left) and ee (right) events. The points with error bars represent the data. The uncertainties on the data points (statistical only) represent 68% confidence intervals for the Poisson means. The filled histograms represent the expectations from SM processes: Z/γ^*, $t\bar{t}$, other sources of prompt leptons (tW, diboson production, $Z \rightarrow \tau\tau$), and the multi-jet backgrounds.

colliding two heavy nuclei at LHC energies one expects to form a hot and dense deconfined medium at energy densities never probed before.

One of the first proposed signatures of QGP formation was "jet quenching" [51] i.e. the attenuation or disappearance of the spray of hadrons resulting from the fragmentation of a hard scattered parton having suffered energy loss in the dense plasma produced in the reaction. The energy lost by a parton in a medium provides fundamental information on its thermodynamical and transport properties. Results from nucleus-nucleus collisions at the Relativistic Heavy Ion Collider (RHIC) have proved conclusively the existence of partonic energy loss in the suppressed single inclusive high-p_T hadron production, and in the modified high-p_T di-hadron angular correlations.

At leading order (LO) and in the absence of parton energy loss in the QGP, the two jets have equal transverse momenta with respect to the beam axis (p_T) and are completely correlated in the azimuthal angle ($\Delta\varphi_{\text{dijet}} = \left|\varphi_{\text{jet1}} - \varphi_{\text{jet2}}\right| \approx \pi$). However, medium-induced gluon emission in the final state can significantly unbalance the energy between the two highest p_T (leading and sub-leading) jets and give rise to deviations of the azimuthal angle between jets from π.

Jet production in lead-lead collisions was studied in CMS as a function of the centrality of the events and the energy of the leading jet [52]. The jet energy imbalance in dijet events is found to be much larger than in proton-proton events, and is increasing with the centrality of the collision. Jets were reconstructed from their energy deposits in calorimeters. In general, the energy loss by partons traversing the medium with different path lengths leads to modifications in the observed dijet energy balance, if the radiated energy falls outside the area used for the determination of the jet energy or if the energy is shifted towards low momentum particles that will not be detected in the calorimetric energy measurement. Such unbalanced events were in fact immediately seen during the very first days of data taking. The apparently unbalanced jet events could be observed

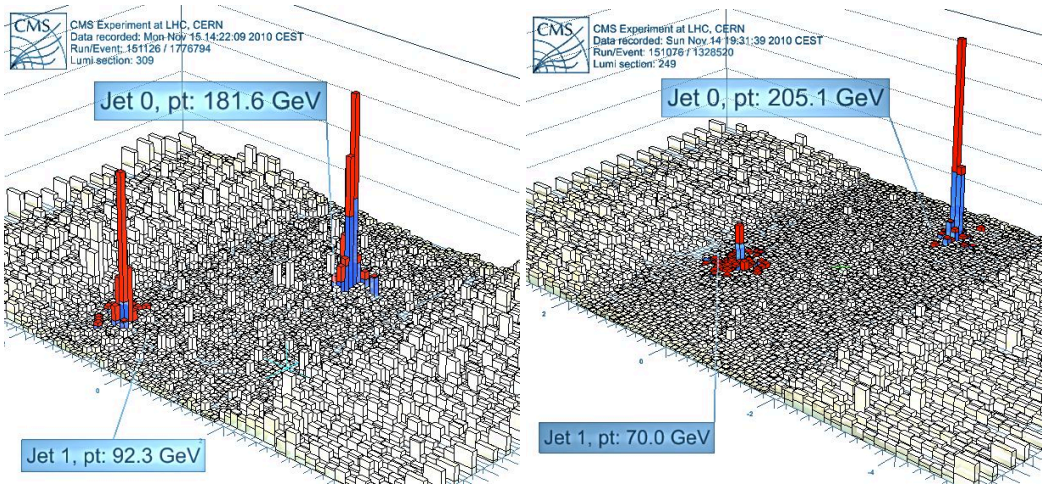

Figure 12: Examples of unbalanced dijet events. The jet energy balance $A_J = \frac{p_{T,1}-p_{T,2}}{p_{T,1}+p_{T,2}}$ is 0.33 for the event shown on the left and 0.49 for the event shown on the right.

by eye on event displays by simply scanning through jet triggered events. Two examples of these such events are shown in Fig. 12.

9.1 Dijet momentum distribution

To characterize the dijet energy balance (or imbalance) quantitatively, we define the asymmetry ratio $A_J = (p_{T,1} - p_{T,2})/(p_{T,1} + p_{T,2})$ where the subscript 1 always refers to the leading jet so that A_J is positive by construction. This asymmetry value was calculated for pairs of jets where the leading jet had $p_{\mathrm{T}} > 120$ GeV/c and the subleading jet had $p_{\mathrm{T}} > 50$ GeV/c There was also a restriction that the jets be separated by $\Delta\phi > 2\pi/3$ (i.e. approximately back-to-back). It is important to note that the use of A_J to a large extent removes uncertainties due to possible constant shifts of the jet energy scale.

Figure 13 shows the fraction of the events as a function of A_J for five bins in centrality (and the inclusive 0-100% selection), comparing the data to reconstructed PYTHIA dijets embedded in data events, with only statistical errors shown. For the most peripheral bins, the data points show similar values to those seen for MC, with only a small shift to larger average asymmetries. As the events become more central, the shape of the A_J distribution for data changes dramatically, while the embedded PYTHIA events show only a modest broadening event for the most central collisions. Dijets found in the most central events show a very significant deficit of events in which the two jets are balanced and a significant excess of unbalanced pairs. This large excess of unbalanced compared to balanced events explains why this effect was apparent already simply by scanning event displays (see Fig. 12). The inclusive 0-100% centrality bins (Fig. 12a)) shows this effect taking the dataset as a whole. Half of the jets produced are in centrality of 0-20%, and the measured imbalance in the central bin shows up strongly on this inclusive plot.

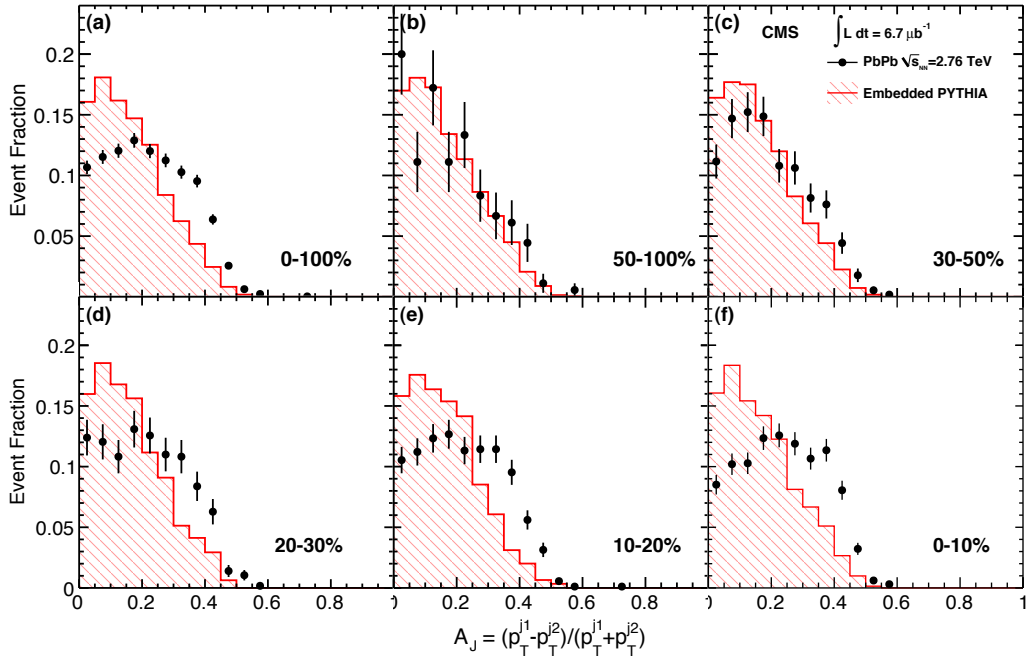

Figure 13: Dijet asymmetry ratio, A_J, for leading jets of $p_{\mathrm{T}} > 120$ GeV/c and subleading jets of $p_{\mathrm{T}} > 50$ GeV/c with a selection of $\Delta\phi > 2\pi/3$ between the two jets. Plots are shown for a) all centralities (0-100%), and in five bins of centrality from peripheral (b) to central (f) collisions. Results from data are shown as black points while the histogram shows the reconstruction of PYTHIA dijets embedded into data events. Error bars shown are statistical.

10. Conclusions

We have described the main CMS physics results obtained by summer 2011. The CMS detector at LHC started collecting data at 7 TeV centre-of-mass energy in 2010. During 2011 the LHC luminosity was increased up to $3 \times 10^{33}\mathrm{cm}^{-2}\mathrm{s}^{-1}$. CMS carried out many QCD and electroweak measurements. No new particles have been detected until now up to a mass of O(1 TeV) and new and more stringent limits have been derived. The allowed Higgs boson mass range has been further restricted compared to the LEP and Tevatron results and the SM Higgs mass ranges 145–216, 226–288, and 310–400 GeV/c^2 have been excluded at 95% C.L. by CMS using an integrated luminosity of 1.6 fb^{-1}. CMS also collected and analyzed 6.7 $\mu\mathrm{b}^{-1}$ of heavy ion interactions (Pb-Pb) at a nucleon-nucleon centre-of-mass energy of 2.76 TeV that allowed to study the properties of quark gluon plasma.

Acknowledgments

We would like to thank first of all the LHC accelerator team for the impressive performance of the machine that allowed us to collect so many data in such a short time. We would also like to give special thanks to the conference organizers for the excellent organization and for giving us the opportunity to presents our results.

References

[1] CMS Collaboration,"The CMS experiment at the CERN LHC", *JINST* **3** (2008) S08004.

[2] M. Cacciari, G. P. Salam, and G. Soyez, "The Anti-k_{T} Jet Clustering Algorithm", *JHEP* **04** (2008) 063.

[3] CMS Collaboration,"Measurement of the Inclusive Jet Cross Section in pp Collisions at $\sqrt{(}s) = 7$ TeV" Phys. Rev. Lett. **1**07 (2011) 132001.

[4] CMS Collaboration,"Measurement of the differential dijet production cross section in proton-proton collisions at $\sqrt{(}s) = 7$ TeV" Phys. Lett. **B**700 (2011) 187.

[5] CMS Collaboration,"Observation of Long-Range, Near-Side Angular Correlations in Proton-Proton Collisions at the LHC" J. High Energy Phys. **0**9 (2010) 091.

[6] E. L. Berger, "Rapidity Correlations at Fixed Multiplicity in Cluster Emission Models", *Nucl. Phys.* **B85** (1975) 61.

[7] A. Morel and G. Plaut, "How Do Clusters Look in Semiinclusive Cross-Sections?", *Nucl. Phys.* **B78** (1974) 541.

[8] K. Eggert et al., "Angular Correlations between the Charged Particles Produced in pp Collisions at ISR Energies", *Nucl. Phys.* **B86** (1975) 201.

[9] L. Foa, "Inclusive Study of High-Energy Multiparticle Production and Two-Body Correlations", *Phys. Rep.* **22** (1975) 1.

[10] UA5 Collaboration, "Charged Particle Correlations in $\bar{p}p$ Collisions at C.M. Energies of 200 GeV, 546 GeV and 900 GeV", *Z. Phys.* **C37** (1988) 191.

[11] PHOBOS Collaboration, "Cluster Properties from Two-Particle Angular Correlations in pp Collisions at $\sqrt{s}$= 200 GeV and 410 GeV", *Phys. Rev.* **C75** (2007) 054913.

[12] PHOBOS Collaboration, "System Size Dependence of Cluster Properties from Two- Particle Angular Correlations in Cu+Cu and Au+Au Collisions at $\sqrt{s_{NN}}$ = 200 GeV", *Phys. Rev.* **C81** (2010) 024904.

[13] B. Alver et al., "System Size, Energy and Centrality Dependence of Pseudorapidity Distributions of Charged Particles in Relativistic Heavy Ion Collisions", *Phys. Rev. Lett.* **102** (2009) 142301.

[14] PHOBOS Collaboration, "High transverse Momentum Triggered Correlations over a Large Pseudorapidity Acceptance in Au+Au Collisions at $\sqrt{s_{NN}}$=200 GeV", *Phys. Rev. Lett.* **104** (2010) 062301.

[15] STAR Collaboration, "Three-Particle Coincidence of the Long Range Pseudorapidity Correlation in High Energy Nucleus-Nucleus Collisions", *Phys. Rev. Lett.* **105** (2010) 022301.

[16] CMS Collaboration,"Measurement of the Inclusive W and Z Production Cross Sections in pp Collisions at $\sqrt{(}s) = 7$ TeV with the CMS experiment" J. High Energy Phys. **1**0 (2011) 132.

[17] CMS Collaboration,"Measurement of Wγ and Zγ production in pp collisions at $\sqrt{(}s) = 7$ TeV" Phys. Lett. **B** 701 (2011) 535.

[18] CMS Collaboration,"WW, WZ and ZZ cross sections", *CMS PAS* EWK-11-010 (2011).

[19] CMS Collaboration,"Top pair cross section in lepton+jets+btag", *CMS PAS* TOP-11-003 (2011).

[20] CMS Collaboration,"Top pair cross section in dilepton channel", *CMS PAS* TOP-11-005 (2011).

[21] CMS Collaboration,"Top pair cross section in hadronic channel", *CMS PAS* TOP-11-007 (2011).

[22] CMS Collaboration,"Top pair cross section in tau dilepton channel", *CMS PAS* TOP-11-006 (2011).

[23] CMS Top Physics Results: https://twiki.cern.ch/twiki/bin/view/CMSPublic/PhysicsResultsTOP.

[24] CMS Collaboration,"Top pair charge asymmetry", *CMS PAS* TOP-11-014 (2011).

[25] CMS Collaboration,"Top quark-antiquark mass difference", *CMS PAS* TOP-11-019 (2011).

[26] CMS Collaboration,"Search for single top production in the tW-channel", *CMS PAS* TOP-11-022 (2011).

singe

[27] A. J. Buras, "Minimal flavour violation and beyond: Towards a flavour code for short distance dynamics", *Acta Phys. Polon. B* **41** (2010) 2487.

[28] CDF Collaboration, "Search for $B_s^0 \to \mu^+\mu^-$ and $B^0 \to \mu^+\mu^-$ Decays with CDF II", (2011) arXiv:1107.2304.

[29] CMS Collaboration,"Search for $B_s^0 \to \mu^+\mu^-$ and $B^0 \to \mu^+\mu^-$ decays in pp collisions at $\sqrt{(}s) = 7$ TeV" Phys. Rev. Lett. **1**07 (2011) 191802.

[30] CMS and LHCB Collaborations, LHCb-CONF-2011-047, *CMS PAS* BPH-11-019 (2011).

[31] S. Weinberg, "A Model of Leptons", *Phys. Rev. Lett.* **19** (1967) 1264.

[32] A. Salam, "Elementary Particle Theory", p. 367. Almquist and Wiksells, Stockholm, 1968.

[33] F. Englert and R. Brout, "Broken symmetries and the masses of gauge bosons", *Phys. Rev. Lett.* **13** (1964) 321.

[34] P. W. Higgs, "Broken symmetry and the mass of gauge vector mesons", *Phys. Rev. Lett.* **13** (1964) 508.

[35] R. Barate and others (LEP Working Group for Higgs boson searches and ALEPH, DELPHI, L3, and OPAL Collaborations), "Search for the standard model Higgs boson at LEP", *Phys. Lett.* **B565** (2003) 61–75.

[36] CDF and D0 Collaborations, "Combined CDF and D0 upper limits on Standard Model Higgs Boson production", (July, 2011). arXiv:1107.5518. CDF Note 10606 and D0 Note 6226.

[37] The ALEPH, CDF, D0, DELPHI, L3, OPAL, SLD Collaborations, the LEP Electroweak Working Group, the Tevatron Electroweak Working Group,and the SLD electroweak and heavy flavour groups, "Precision Electroweak Measurements and Constraints on the Standard Model", *CERN-PH-EP-2010-095, http://lepewwg.web.cern.ch/LEPEWWG/plots/summer2010/, http://arxiv.org/abs/1012.2367* (2010).

[38] CMS Collaboration, "Search for a Higgs boson decaying into two photons in the CMS detector", *CMS PAS* HIG-11-021 (2011).

[39] CMS Collaboration, "Search for a Standard Model Higgs boson in the decay channel $H \to ZZ^{(*)} \to 4\ell$", *CMS PAS* HIG-11-015 (2011).

[40] CMS Collaboration, "Search for the Higgs Boson Decaying to W^+W^- in the Fully Leptonic Final State", *CMS PAS* HIG-11-014 (2011).

[41] CMS Collaboration, "Search for standard model Higgs boson in pp collisions at $\sqrt{s} = 7$ TeV and integrated luminosity up to 1.7 fb^{-1}", *CMS PAS* HIG-11-022 (2011).

[42] M. Drees and M. M. Nojiri, Phys. Rev. **D** 47 (1993) 376.

[43] G. L. Kane, C. Kolda, L. Roszkowski and J. D.Wells, "Study of constrained minimal supersymmetry", Phys. Rev. **D** 49 (1994) 6173.

[44] CMS Exotica Physics Results: https://twiki.cern.ch/twiki/bin/view/CMSPublic/PhysicsResultsEXO.

[45] CMS Collaboration "Search for Resonances in the Dilepton Mass Distribution in pp Collisions at sqrt(s) = 7 TeV", *CMS PAS* EXO-11-019 (2011).

[46] F. Karsch and E. Laermann, "Thermodynamics and in-medium hadron properties from lattice QCD", arXiv:hep-lat/0305025.

[47] E. V. Shuryak, "Theory of Hadronic Plasma", *Sov. Phys. JETP* **47** (1978) 212–219.

[48] J. C. Collins and M. J. Perry, "Superdense Matter: Neutrons Or Asymptotically Free Quarks?", *Phys. Rev. Lett.* **34** (1975) 1353.

[49] N. Cabibbo and G. Parisi, "Exponential Hadronic Spectrum and Quark Liberation", *Phys. Lett.* **B59** (1975) 67–69.

[50] B. A. Freedman and L. D. McLerran, "Fermions and Gauge Vector Mesons at Finite Temperature and Density. 3. The Ground State Energy of a Relativistic Quark Gas", *Phys. Rev.* **D16** (1977) 1169.

[51] J. D. Bjorken, "Energy loss of energetic partons in QGP:possible extinction of high pT jets in hadron-hadron collisions", FERMILAB-PUB-82-059-THY.

[52] CMS Collaboration "Observation and studies of jet quenching in PbPb collisions at $\sqrt{(}s) = 2.76$ TeV" Phys. Rev. **C** 84 (2011)